Drying of green veneer hollow tubes monitored using stereo digital images correlation

Citra Yanto Ciki Purba[1] · Joffrey Viguier[1] · Louis Denaud[1] · Bertrand Marcon[1] · Régis Pommier[2]

Abstract

The present study is based on the patent FR3052379A1, which consists of rolling and gluing green veneers to form structural size hollow tubes. The objective was to study the drying behavior of circular hollow tubes and investigate the method of crack detection using image correlation from green conditions to equilibrium moisture content. The manufactured tubes are composed of six plies. Three different configurations of global grain angle orientations with respect to the tube longitudinal axis are used: $\{0, 0, 0\}°$, $\{10, 0, 10\}°$, and $\{-10, 0, 10\}°$. Each grain angle was made up of two plies. The tubes deformation and crack formation due to drying shrinkage were measured using a stereo digital image correlation system. The stereo correlation is suitable for measuring tangential shrinkage and studying the opening and/or closing of cracks on the surface of the tubes subjected to internal moisture variations and blocked deformations. The influence of grain angle was discussed in this paper; however, due to the very few numbers of samples, no conclusive findings can be made.

1 Introduction

The manufacture of hollow core lumber makes it possible to obtain more efficient cross-sectional shapes that provide lighter structural elements and to manufacture dimensions that are not currently available in sawn timber. Various types of hollow woods are available on the market; some are made of solid wood and others are made of veneer. The circular hollow structure is one of the most studied shapes, especially for its mechanical property and its potential for energy absorption. Farley and Jones (1992) studied the crushing response of fiber-reinforced composite tubes. Hartig et al. (2018) performed research on the lateral vehicle impact equipped with beech and a fiber glass reinforced beech tube. A more recent study by Guélou et al. (2021) reported the potential use of tubes made of poplar veneer for crash applications and their peculiar energy absorption potential. The present study is based on a patent related to an additive manufacturing process that consists of rolling and gluing green veneers to form cylindrical tubes (Pommier et al.

2017). Additive manufacturing technology is growing in all sectors of the material industry, including the wood industry. Recent studies show that hollow tubes made from veneers can be used for structural elements such as beams, utility poles, and soil reinforcement nailing systems (Hirschmüller et al. 2019; Gilbert et al. 2020). Hirschmüller et al. (2019) have reported the tensile and bending properties of circular hollow sections made of beech LVL (laminated veneer lumber) under various periods of immersion in a water–cement grout solution. Gilbert et al. (2020) presented a numerical model to capture the structural response of timber circular hollow sections loaded in bending.

Except for very specific cases such as thin veneers and when using a high nosebar pressure, peeled veneers present lathe checks on their loose surface as described in Fig. 1a. The presence of these lathe checks makes it easier to bend the veneer. For a given species and a fixed thickness, their depth and frequency are mostly dependent on the log steaming temperature and the pressure rate of the pressure bar (Rohumaa et al. 2018; Purba et al. 2019). Purba et al. (2019) reported that for 2.1 mm thick beech veneers, the average depth of lathe check is 46.3%, representing almost half the thickness of the veneer. Plasticisation due to high moisture content (MC) and high temperature for fabrication of green veneer also makes it possible to bend and form various shapes without damaging their integrity as it induces a plasticization process that softens the bond

✉ Citra Yanto Ciki Purba
  purbacitrayantociki@gmail.com

1 Arts et Metiers Institute of Technology, LaBoMaP, HESAM Université, 71250 Cluny, France

2 Univ. Bordeaux, I2M, UMR 5295, 351 Cours de la Libération, 33400 Talence, France
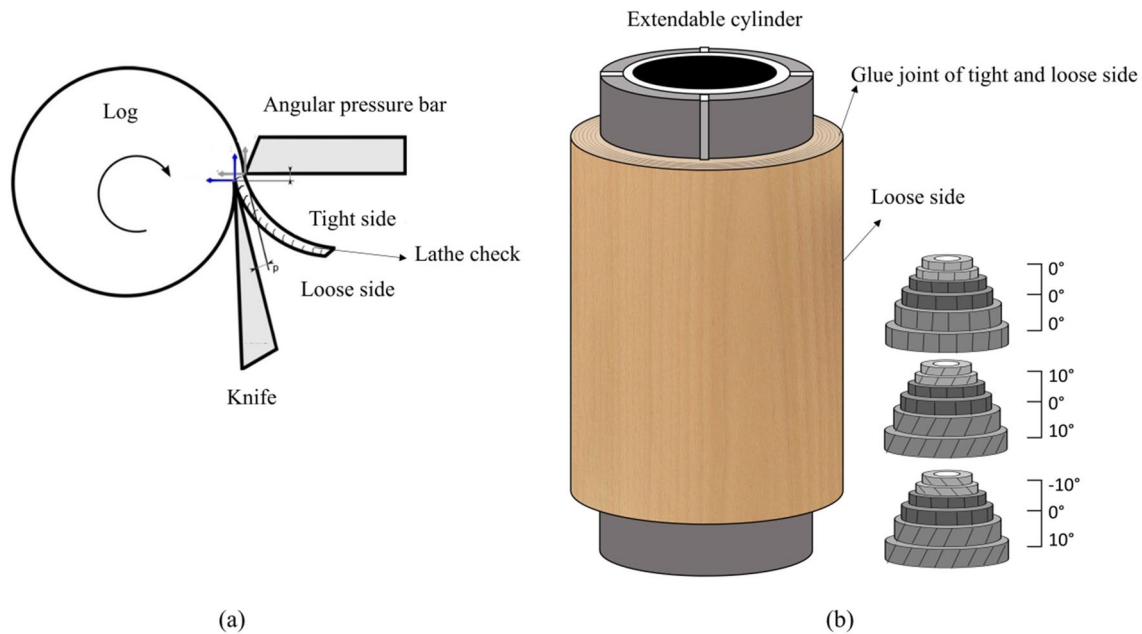
Fig. 1 **a** Diagram of rotary peeling process and the location of lathe checks, **b** hollow tube assembly with all three different configurations of the grain angle used

between hemicelluloses and lignin (Kollmann 1955; Bader and Nemeth 2019). Recent studies on *Mansonia altissima* and *Pinus pinaster* show that it is possible to manufacture plywood from green veneers using polyurethane (PUR) (Lavalette et al. 2016; Makomra et al. 2020). This material forming method could be used to fabricate curved panels for automotive parts or to mold directly boat structures.

Lavalette et al. (2016) have shown positive results for the structural use of green-glued wood. However, during the drying, cracks are generated on the surface of the plywood. Cracks are generated during drying since the shrinkage stresses can exceed the tensile strength of the material, which results in locally weakening of the area near a lathe check. These cracks occur in the longitudinal direction and are caused by internal stresses created during drying by the difference between the drying rate of the wood in the tangential and radial directions and by the gradients of moisture content (Langrish and Bohm 1997; Pang 2000) within the tube thickness. The tangential shrinkage is generally twice as high as the radial shrinkage ratio in most wooden species. On the other hand, the moisture content gradients are created when one surface of the wood dries faster than the opposite one (Sepulveda-Villarroel et al. 2016). It is important to note that the presence of cracks may reduce the durability by giving access to moisture, fungi and insects to penetrate the inner part of the structure. However, some studies have shown that the presence of cracks does not have a significant impact on the structural behavior of the whole timber as cracks appear mostly parallel to the axis of the

tube and therefore do not affect too much its mechanical performances in the axis (pure tension–compression) but they can be more penalizing for off-axis stresses such as shear stress (Huybers 1987; Eckelman 2004). Therefore, avoiding the generation and growth of the crack is a challenge to overcome based on the experimental information and the optimization process. Vacuum drying with cycles of drying and humidification has been proposed as one of the solutions to minimize crack formation. These cycles activate the viscoelastic and hygroelastic relaxation phenomena so that the stresses due to wood shrinkage do not cause damage (Makomra et al. 2020).

Crossing the orientation of the plies, which constructs the LVL, may also reduce the surface checks as the cross-oriented veneers prevent the propagation of cracks generated in the close-by layers. However, the deviation of the fiber orientation could cause a distortion of the hollow tube shape when the tube dries. According to the literature, the grain angle format of LVL {0, 0, 0}° and plywood {0, 90, 0}° give the best shape stability on a molded product (Blomqvist et al. 2013). Adding cross-oriented layers to the LVL is a common practice in order to increase dimensional stability. Nevertheless, the grain angle also influences the mechanical properties. The mechanical properties such as the bending properties are decreasing with rising grain angle (Hamada et al. 1996; Barnes 2002).

The present work aimed to study the drying behavior of circular hollow tubes and to investigate the method of crack detection using image correlation. Digital image correlation

(DIC) is increasingly used to measure surface deformations on flat surfaces of wood (Valla et al. 2011; Peng et al. 2012; Lanvermann et al. 2014; Rosero-Alvarado et al. 2018; Garcia et al. 2020; Pang and Jeong 2020; Sutton et al. 2009; Viguier et al. 2021). Valla et al. (2011) used DIC-2D to measure the in-plane deformation on mechanically stressed plywood. Lanvermann et al. (2014) used neutron imaging (NI) to detect water and DIC-2D to measure the local deformation in order to study the intra-ring moisture variation in Norway spruce. Pang and Jeong (2020) also studied the swelling and shrinkage behaviors of cross-laminated timber (CLT) using DIC-2D. The DIC-2D cannot be used on non-flat surfaces, such as the tube is, which is why its three-dimensional version is used in the present study. DIC-3D or stereo-DIC has been used by Rosero-Alvarado et al. (2018) to measure the surface deformation of walnut burl veneer on aircraft sandwich panels. In addition, Shao et al. (2016) also used DIC-3D to measure deformation on large engineering components. A recent study using DIC-2D shows that it can be used to study the development of checks on the veneer surface and to measure checks as narrow as 0.2 mm wide with a precision of 0.03 mm (Burnard et al. 2018). Thus, the drying behavior of green veneer hollow tubes was studied here with the help of stereo digital image correlation (DIC-3D) to calculate the displacements and strains on the surface of the hollow tube. The circular green tubes were fabricated using PUR. Previous studies have shown that PUR is suitable for green wood gluing (Properzi et al. 2003; Lavalette et al. 2016). PUR requires adequate proportion of water and adhesive in order to get enough water to react with the prepolymer of polyurethane and to have enough adhesive to create bonds with the wood cell wall components.

2 Method

2.1 Hollow tubes fabrication

In this study, three beech logs were rotary peeled utilizing common process parameters. These logs were soaked at a temperature of 65 °C for 24 h prior to peeling. The beech logs were peeled into 2 mm thick veneers (i.e. the thickness at green state) using the peeling lathe SEM-S500 equipped with a 900 mm long knife. The linear cutting speed was set at 1.5 m/s and the pressure rate of the angular pressure bar was adjusted to 10%, which corresponds to a gap of 1.8 mm (90% of the expected green veneer thickness) between the knife and the pressure bar.

The tight surface of the freshly cut beech veneer was first covered with polyurethane (PU) glue. A glue spread of 140–180 mm^2 was requested by the manufacturer for gluing wood with minimum MC 8% and maximum 18%. The glue quantity used in this study was about 250 g/m^2, as reported

in the literature on green gluing of veneer (Lavalette et al. 2016), due to the fact that a larger quantity of glue is better for wood gluing using PUR above the fiber saturation point (FSP) or 30% MC (Pröller 2016). The green veneers were then rolled on a radially expanding cylinder. The unloaded radius of the cylinder was 110 mm and could be extended up to 115 mm when compressed air is injected into the cylinder. The pressure of the compressed air injected into the cylinder was set at 4 bars.

The manufactured hollow tubes were composed of six plies as presented in Fig. 1b. Three veneer sheets of different lengths were arranged in accordance with the circumference of the cylinder; each veneer sheet being long enough to cover two revolutions of the tube. To study the influence of the grain angle on the drying behavior of the LVL tube, three different configurations of the grain angle were used. The first configuration was {0, 0, 0, 0, 0, 0}° which corresponds to a straight-grained hollow tube (grain orientation parallel with the tube axis). The second configuration was {10, 10, 0, 0, 10, 10}° corresponding to parallel orientation of the inner and outer veneer surfaces. The third configuration used was {− 10, − 10, 0, 0, 10, 10}° where the inner and outer veneer surfaces were oriented crosswise. Since each veneer sheet was rolled twice around the cylinder, the three configurations are referenced as: {0, 0, 0}, {10, 0, 10}, and {− 10, 0, 10}. The 10° angle of the cross veneer has been chosen to ensure that the veneer can be rolled up; a higher angle requires much larger veneers and is difficult to roll up. It should be noted, however, that rolling up the veneer on the expanding cylinder may slightly change the actual grain angle with respect to the longitudinal direction of the tube, despite the precautions taken during processing. A plastic sheet and adhesive tape were then placed over the entire surface of the laminated veneer to maintain the MC of the veneer and to hold the laminated veneer together during the pressing process. In addition to the suitability of PUR for high MC gluing, PUR is also compatible with low pressure gluing. The pressure was maintained for 24 h to allow the adhesive to cure. Once the pressing process was completed, the LVL tubes were then cut to the final length of 500 mm. Three tubes were fabricated, thus one tube for each configuration. The image of a finished product is presented in Fig. 2.

2.2 DIC setup and measurement

The hollow tube, which was still in the green state, was then placed on a scale and dried in the open air. The relative humidity and the temperature of the room is presented in Table 1. A support made of perforated metal was placed between the tube and the scale which allows the bottom of the tube to dry without any restriction (air exchanges and movements not affected). By monitoring the mass loss during the drying, the average MC of the tube is deduced

**Fig. 2** Circular hollow tube made of green beech veneer

Table 1 Average relative humidity and temperature of the room during drying of circular hollow tubes for each grain angle configuration

Air parameter	Grain angle configuration		
	{0, 0, 0}	{10, 0, 10}	{−10, 0, 10}
Mean temperature (°C)	21 ± 1.5	21 ± 0.7	21 ± 0.5
Mean relative humidity (%)	42 ± 3	35.33 ± 1.0	39 ± 1.5

as a function of the drying time. The mass loss was monitored using an analytical scale Sauter RC-8021 with 0.1 g resolution.

The drying deformations (shrinkage) of the hollow tube due to moisture loss in all directions were measured using a LaVision StrainMaster stereo image correlation system (DIC-3D). This system consists of two CCD cameras and LED projectors that are synchronized with the image capture. The CCD cameras used were Imager M-lite with 35 mm lenses (Nikon AF-S NIKKOR). The distance between the cameras and the hollow tube was 1300 mm. The image resolution was 4096 × 2168 pixels and the spatial resolution was 0.22 mm/pixels. Facet size (window sizes) of 41 pixels and facet step (window step) of 13 pixels were applied to the correlation computation. The setup for the experiment is presented in Fig. 3.

The fundamental basis of DIC is tracking a pattern in a sequence of images. Therefore, to obtain accurate measurements of deformation, the DIC technique requires high contrast and a random pattern of uniformly sized speckles on the measured surface. Black speckles were applied to the hollow tube surface directly after pressing. Every hour, the DIC-3D system took an image of the hollow tube and the scale. The measurements for each of the three hollow tubes were taken over a period of 10 days or until the hollow tube reached at least 15% MC. At the end of the experimental campaign, the hollow tube was then dried in an oven at 103 ± 2 °C for 48 h to determine its anhydrous mass, allowing the average internal MC levels to be calculated afterward.
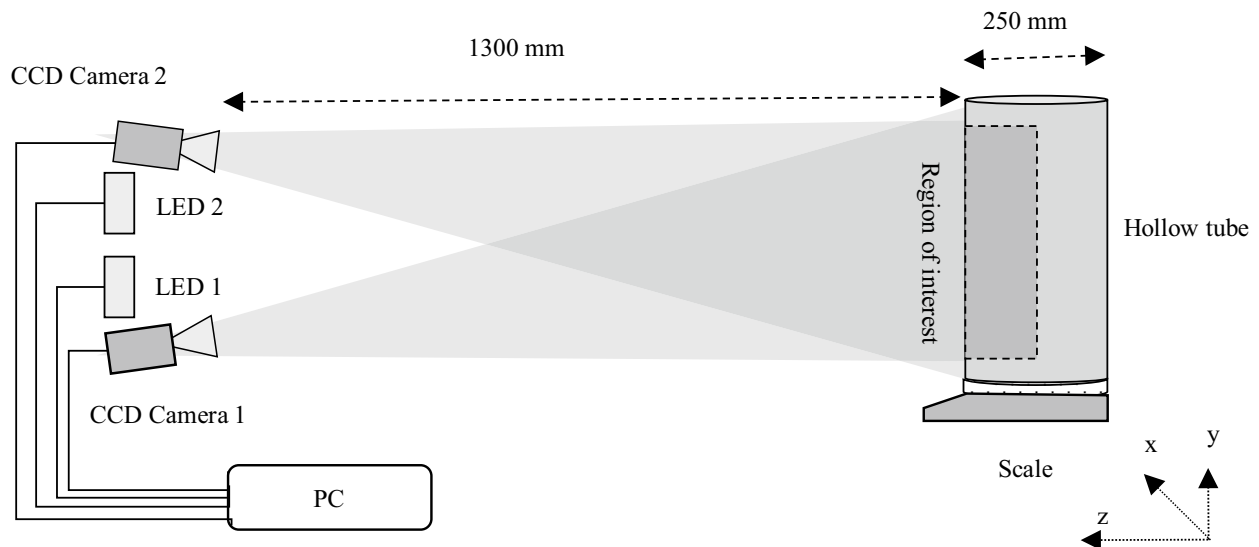
Fig. 3 Schematic of the experimental setup. CCD cameras 1 and 2 were inclined 9° and 25° respectively towards the hollow tube. The region of interest dimension was 400 mm × 250 mm in y and z directions (plane measured)

2.3 Data analysis

The local tangential shrinkage (Ts) was defined as the change of distance between two adjacent points (tracked pair of points) in the tangential direction over the initial dimension at the green state and calculated using Eq. 1.

$$Ts = \frac{\sqrt{(x_2 - x_{1)}^2 + (z_2 - z_{1)}^2} - \sqrt{(x'_2 - x'_{1)}^2 + (z'_2 - z'_{1)}^2}}{\sqrt{(x_2 - x_{1)}^2 + (z_2 - z_{1)}^2}} \times 100 \tag{1}$$

where (x_1, z_1) is the coordinate of the first point in the first image, (x_2, z_2) is the coordinate of the second point in the first image, (x'_1, z'_1) and (x'_2, z'_2) is the coordinate of those respective points in the second image (after $\Delta t = 1$ h). The average tangential shrinkage ($\overline{Tsp}$) was calculated from the local tangential shrinkage by excluding the negative values (Eq. 2). Indeed, a negative local shrinkage means that the distance between two measured points became further away instead of getting closer with the decrease in MC which can be the signature of a local crack. The tangential shrinkages between -0.5% and 0.5% thresholds were excluded from all computations since it embeds the DIC pseudostatic accuracy (i.e. residual minimum and maximum strains from processing the autocorrelation of images freed of strains); this $[-0.5;0.5]\%$ Ts range could be considered as strain determination error. Indeed, identifying negative and positive tangential strains without taking into account the DIC measurement limitations leads to total miscalculations of their proportions over the surfaces of the tube.

To describe the effect of the drying process on the check splitting or growing considering the effect of the veneer orientation, three indicators were built taking into account only these negative local tangential shrinkage values. The calculation of the average negative shrinkage ($\overline{Tsn}$) value was performed as presented in Eq. 2 as an indication of the crack width:

$$\overline{Tsp} = \frac{\sum_{i=1}^{N} Tsp_i}{N} \text{ and } \overline{Tsn} = \frac{\sum_{i=1}^{N} Tsn_i}{N} \tag{2}$$

The proportion of negative shrinkage ($PTsn$) was calculated as the ratio of the number of negative values to the total number of measured local tangential shrinkage (Eq. 3). The proportion of negative shrinkage was calculated to represent the percentage of the veneer surface area with cracks over the measured surface area of the hollow tube (considering that the observation area is wide enough to figure the whole hollow tube behavior). Area with cracks mentioned earlier means area with negative tangential shrinkage, which includes both area with and without wood on the tube surface.

$$PTsn = \frac{Area\ with\ negative\ shrinkage}{Total\ measured\ area} \tag{3}$$

The intensity of the checks (IC) was then calculated as the average tangential shrinkage divided by the proportion of negative shrinkage, as presented in Eq. 4. The calculation of the intensity of the checks allowed us to compare the severity of the cracks on the three configurations of hollow tubes.

$$IC = \frac{\overline{Tsn}}{PTsn} \tag{4}$$

The tube's shape stability analysis was evaluated in comparison with the perfectly cylindrical shape of the hollow tube along with the moisture changes while drying based on the stereo correlation data (x and z positions). This analysis was based on the decomposition of the tube cross-section (transversal plane) into segments as presented in Fig. 4a, b and calculation of the angle θ between two adjacent points to the reference point (x = 0) using the atan2 mathematical operator as presented in Eq. 5. In trigonometry, the function atan2 is simply a variation of the arctangent function; for any real arguments, and for x and z coordinates not both equal to zero, atan2(x, z) is the angle (in radians) between the positive x-axis of a plane and the point given by the coordinates (x, z) on it. To resume, the angle θ provided by the atan function is positive for counter-clockwise angles (upper half-plane, z > 0), and negative for clockwise angles (lower half-plane, z < 0).

$$\theta_i = atan2\left(\frac{z_{i+1} - z_i}{x_{i+1} - x_i}\right) \times \frac{180}{\pi} \tag{5}$$

where θ is the angle between two consecutive segments of the discretized tube external perimeter, x_i and y_i are the coordinates of the considered segment endpoint. Figure 4c provides the evolution of the angle θ when calculated on a perfect circular shape. As can be seen, the atan2 function of a circle delivers an almost linear trend. The x distance between the two consecutive points of the perimeter is regular and fixed at 2 mm (arising from the DIC settings). The root mean square error (RMSE) of the angles between the dried tube (ranging from 15 to 60% MC) and the green tube (the first stereo DIC measurement) was then calculated and used to evaluate the similarity and the distortion of the tube shape.

Figure 4c was modeled based on a perfectly circular shape which can be used as a reference to determine the angle profile to be expected if the fabricated tubes keep their initially global shape while drying or if they experience distortions; it allowed to check whether the final shape after room conditions equilibrium MC is reached is far from the expected cylinder.
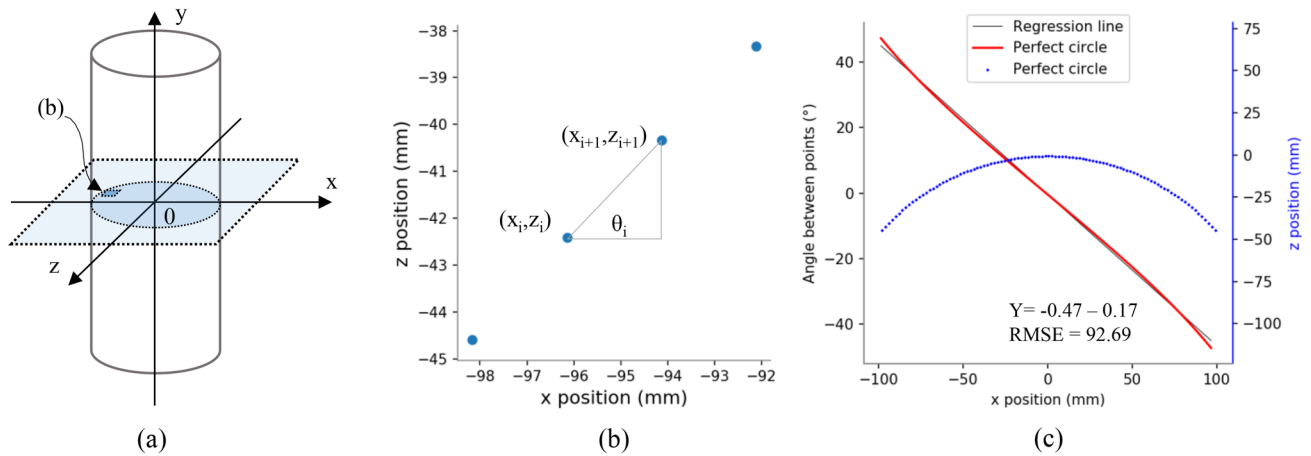
Fig. 4 **a** Positioning of the measuring point on the tube surface, **b** calculation of the angle (θ) between two adjacent points on the surface of the tube, **c** angular profile of a perfectly circular quarter-circle with a diameter of 240 mm and regular × discretization distance between two consecutive points of 2 mm

3 Results and discussion

3.1 Global tangential shrinkage

Figure 5a shows the changes of hollow tube MC as a function of time in the open air while Fig. 5b shows the evolution of the tangential shrinkage *Ts* with the global MC. The hollow tube shrinkage measurement was performed from approximately 60 to 15% MC. It appears that the tangential shrinkage of the hollow tube starts well above the theoretical FSP of beech wood of 32% (Gérard et al. 2011). It seems that a moisture gradient exists through the thickness of the hollow tube. Undeniably, the surface of the hollow tube dries first while the inside plies are still wet and shrink later. As a result, tangential shrinkage of the hollow tube

begins before the average MC of the entire piece is below the FSP. Wood shrinkage, which begins around the FSP, is usually measured in small pieces of wood, making the shrinkage relatively uniform. The influence of specimen size on swelling and shrinkage has been reported in several studies (Stöhr 1988; Peng et al. 2012; Lee and Jeong 2018; Lee et al. 2019). In some recent studies that have measured the shrinkage using more advanced technology, however, it was shown that the dimensional changes in hardwoods such as beech, and softwoods such as red pine, start above the FSP or around 42–50% of MC (Han et al. 2016; Nopens et al. 2019). Such recent studies investigated the shrinkage using DIC, NIRS (near-infrared spectroscopy), and a gravimetric sorption system on small clear specimens with thickness less than 20 mm. Nevertheless, the value presented here was calculated from the local shrinkage profile.

Fig. 5 **a** Evolution of hollow tube MC as a function of time in the open air. **b** Tangential shrinkage measured by stereo image correlation as a function of global internal MC for all 3 hollow tube configurations
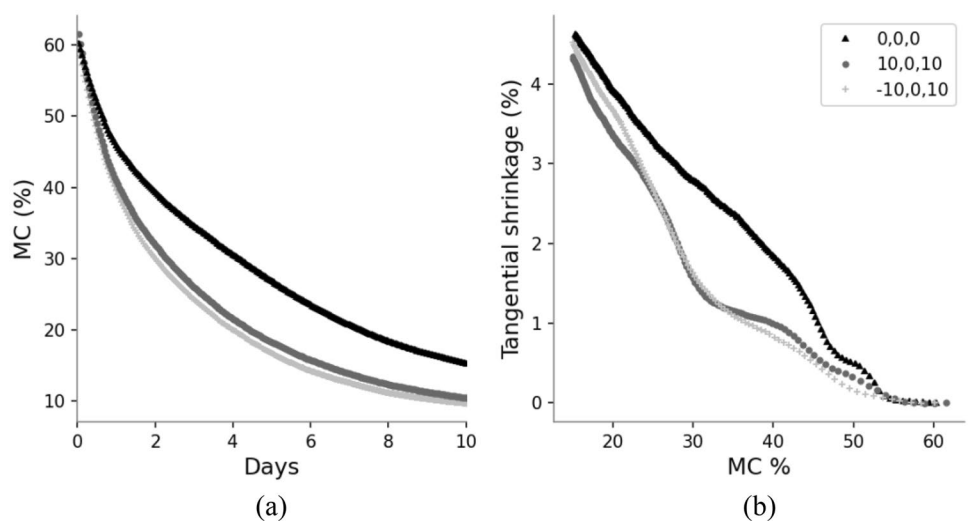
The kinetic of the MC variation in these three stacking configurations was different, which could be due to the drying conditions as presented in Table 1. Those conditions slightly changed since the experiments were made at different moments and without room environmental regulation (air-dried) as exposed in Fig. 5a. The mean room temperature for all three tubes tested was around 21 °C. The mean relative humidity, however, varied from 35% for tube {10, 0, 10} up to 42% for tube {0, 0, 0}. Indeed, the actual shape of the shrinkage curve with moisture changes depends on numerous variables such as the size and shape of the piece, the wood species, and the drying conditions used (Ross 2010). Figure 5b also shows that at 15% MC, the highest tangential shrinkage was found in the {0, 0, 0} tube. However, the actual total tangential shrinkage at 0% MC was not measured in this study. Among all the three configurations, the {10, 0, 10} tube shows the lowest tangential shrinkage at 15% MC.

3.2 The development of the check

Figure 6a shows a map of the local shrinkage values of the hollow tube {0, 0, 0} at 30% MC. The figure is presented as a flattened tube to facilitate the comparison of the local shrinkage profile. The area colored from white to gray corresponds to the surface where the tangential shrinkage was negative, or in other words the locations where the cracks appeared on the surface. This was confirmed by superposing the image of the observed hollow tube surface with the deformation data in Fig. 6b. In previous studies, the presence of checks on the veneer surface was generally detected by

the peak and valley of the strain (Kang et al. 2011; Burnard et al. 2018). It should be noted that the surface cracks started to open after about ten hours of air-drying, which means that the surface of the hollow tube started to dry as soon as it is placed in ambient conditions.

To quantify the presence of these cracks with decreasing MC, the three parameters derived from the tangential shrinkage are calculated according to Eqs. 2, 3, and 4 and are presented in Fig. 7. From this figure, it can be seen that the hollow tube with configuration {0, 0, 0} has the highest average negative shrinkage. In addition, the proportion of negative shrinkage is also highest at the hollow tube with configuration {0, 0, 0}. The lowest of both parameters was found on the hollow tube with configuration {10, 0, 10}.

In this study, the intensity of the checks was considered as the reflection of the crack opening with the reduction in the global hollow tube MC. Figure 7c confirms that the cracks started to open when the MC fell towards the theoretical FSP and then reached the maximum value but then closed again when the moisture fell further below the theoretical FSP, which could indicate a balance of moisture in all parts of the hollow tube. From Fig. 7, we can also see that there were more cracks present on the hollow tube {0, 0, 0} surface than on the other two configurations. Therefore, the hollow tube manufactured with the configuration parallel to the veneer fibers generated high amounts of cracking. It was also noted that the hollow tube of the {10, 0, 10} configuration showed the lowest overall cracking intensity. From these results, the use of a DIC-3D system in wood drying can assess accurately the tangential shrinkage and the presence of cracks on the wood surface. A crack opening, even

(a) (b)
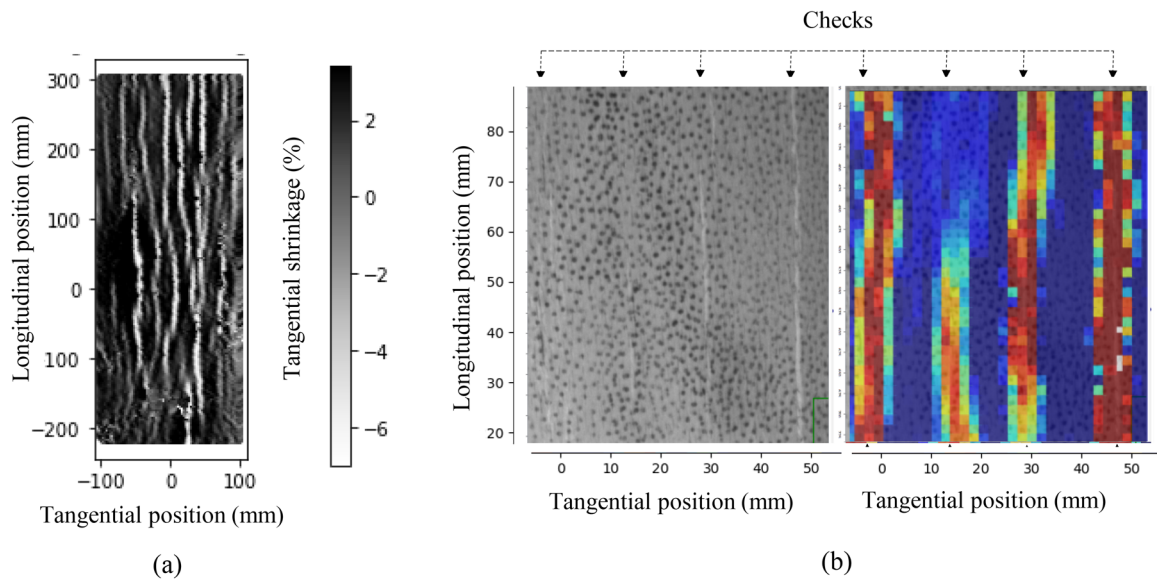
Fig. 6 **a** Map of the local tangential shrinkage on the surface of the flattened tube {0,0,0}, **b** local tangential shrinkage on a part of the observed surface and its correspondence with the location of the cracks in the hollow tube which are marked by arrows
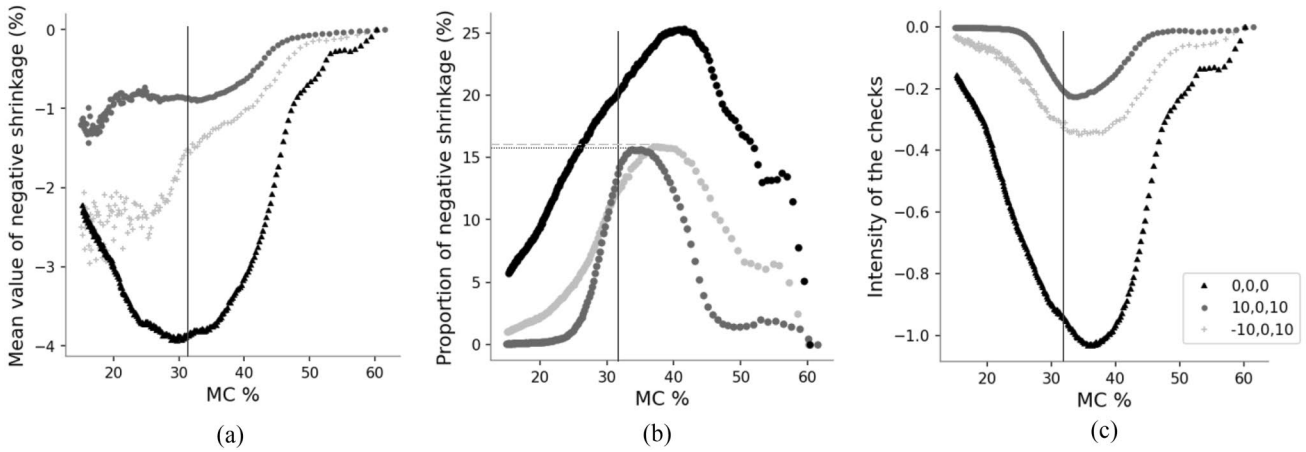
Fig. 7 Comparison of **a** the mean value of negative shrinkage, **b** the proportion of negative shrinkage over the entire surface observed by DIC-3D, **c** the intensity of cracks (mean value/proportion of negative shrinkage) of the three plies stacking configurations. The dashed line represents the theoretical FSP of beech (32% MC)

if it is resealed, can be considered as deterioration and could reduce the mechanical properties of the hollow tube.

It has been shown in the literature that air drying of whole timber generally appears to produce more checks than kiln drying (Bekele 1994). High temperature kiln drying has proven to be more effective than conventional kiln drying in reducing checks, although it also decreases the strength of whole timber structure (Ranta-Maunus 1999). A study by Park et al. (2014) on the drying of center cored whole timber shows that adding a vapor barrier such as a polyethylene wrap to the exterior of cored whole timber during drying, reduces the longitudinal checking to apparently almost none compared to the one without. The vapor barrier establishes an inverted moisture gradient during drying

which counteracts the stresses induced by the difference in tangential vs. radial shrinkage rates. Therefore, a suitable drying schedule or drying technique may help to limit cracking. For the fabrication of circular hollow tubes, however, vacuum drying with humidification cycle seems to have more potential (Makomra et al. 2020).

3.3 Shape stability

Figure 8a, b show that the circular shape of the cross-section of the tube fluctuated with the MC while drying. Figure 8c shows the RMSE variation referenced to the circular shape of the first stereo DIC measurement over various moisture contents. It can be seen that the tube {− 10, 0, 10} gave the
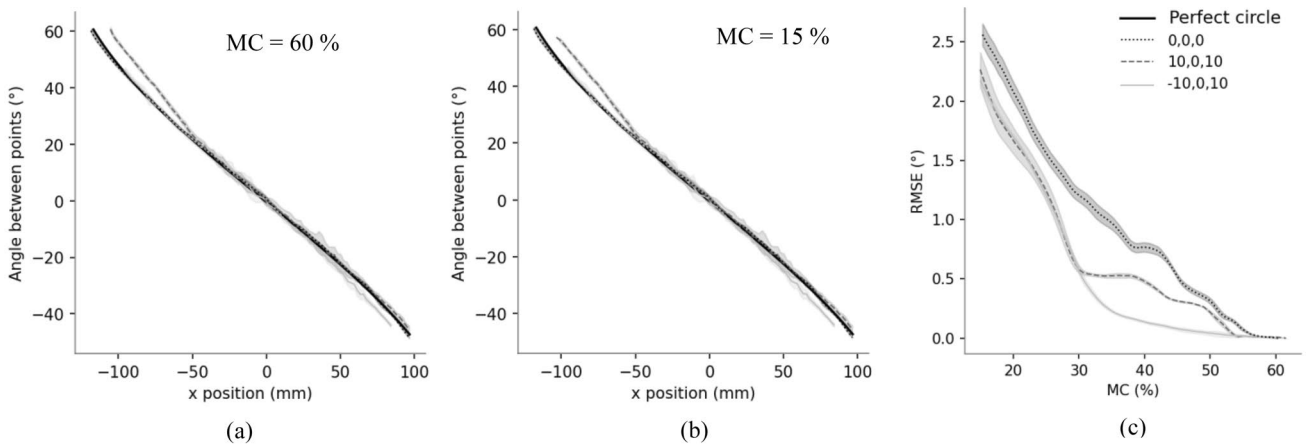
Fig. 8 **a** Reference angle variations of the segments composed of two adjacent points over a cross-section measured on the surfaces of the tubes at 60% MC (green condition), **b** measured at 15% MC (dry), **c** evolution of the angle variation (RMSE) related to the first measurement (green tube) with the MC changes. The solid line and the light color area around each solid line represent the mean value and the standard deviation, respectively

lowest RMSE variation. Therefore, the configuration {−10, 0, 10} generated the best tube shape stability compared with the other two tubes. The tube configuration {0, 0, 0} showed the greatest variation of RMSE with MC changes. In addition, the tube configuration {0, 0, 0} also showed the most scattered values, and thus exhibited the worst shape stability. Crossing the plies, even by only 10°, seems to provide more stability to the circular shape.

4 Conclusion

The DIC-3D appears suitable for measuring tangential shrinkage and studying the opening and/or closing of cracks on the surface of hollow tubes subjected to internal MC variations, but certainly also to observe deformations due to mechanical loading. The cracks on the tube surface started to open when the MC fell towards the theoretical FSP and then reached the maximum value but then closed again when the moisture fell further below the theoretical FSP, which could indicate a balance of moisture in all parts of the hollow tube. The circular shape of the cross-section of the tube fluctuated with the MC while drying. The influence of grain angle has been discussed in this paper. However, due to the insufficient sample size, no conclusive findings can be made. The development of a numerical model could provide a solution to find the optimum angle that provides the best shape stability while maintaining good mechanical properties, but this would only be possible if the model included the real local fiber orientations of the veneers.

References

Bader M, Nemeth R (2019) Moisture-dependent mechanical properties of longitudinally compressed wood. Eur J Wood Prod 77:1009–1019. https://doi.org/10.1007/s00107-019-01448-1

Barnes D (2002) A model of the effect of strand angle and grain angle on the strength properties of oriented veneer and strand wood composites. For Prod J 52:39

Bekele T (1994) Kiln drying of sawn boards of young *Eucalyptus globulus* Labill. And *Eucalyptus camaldulensis* Dehnh. grown on the Ethiopian Highlands. Holz Roh Werkst 52:377–382

Blomqvist L, Johansson J, Sandberg D (2013) Shape stability of laminated veneer products–An experimental study of the influence on distortion of some material and process parameters. Wood Mat Sci Eng 8:198–211

Burnard MD, Muszyński L, Leavengood S, Ganio L (2018) An optical method for rapid examination of check development in decorative plywood panels. Eur J Wood Prod 76:1367–1377. https://doi.org/10.1007/s00107-018-1327-7

Eckelman CA (2004) Exploratory study of high-strength, low-cost through-bolt with cross-pipe and nut connections for square and roundwood timber frame construction. For Prod J Index 54:29–37

Farley GL, Jones RM (1992) Crushing characteristics of continuous fiber-reinforced composite tubes. J Compos Mater 26:37–50

Garcia RA, Rosero-Alvarado J, Hernández RE (2020) Full-field moisture-induced strains of the different tissues of tamarack and red oak woods assessed by 3D digital image correlation. Wood Sci Technol 54:139–159. https://doi.org/10.1007/s00226-019-01145-5

Gérard J, Guibal D, Paradis S et al (2011) Tropix 7. CIRAD. https://doi.org/10.18167/74726f706978

Gilbert BP, Dias-da-Costa D, Lebée A, Foret G (2020) Veneer-based timber circular hollow section beams: behaviour, modelling and design. Constr Build Mater 258:120380. https://doi.org/10.1016/j.conbuildmat.2020.120380

Guélou R, Eyma F, Cantarel A, et al (2021) Crashworthiness of poplar wood veneer tubes. International Journal of Impact Engineering 147:103738

Hamada H, Ramakrishna S, Sato H (1996) Effect of fiber orientation on the energy absorption capability of carbon fiber/PEEK composite tubes. J Compos Mater. https://doi.org/10.1177/002199839603000806

Han Y, Park Y, Park J-H et al (2016) The shrinkage properties of red pine wood assessed by image analysis and near-infrared spectroscopy. Drying Technol 34:1613–1620

Hartig JU, Facchini S, Haller P (2018) Investigations on lateral vehicle impact on moulded wooden tubes made of beech (*Fagus sylvatica* L.). Constr Build Mater 174:547–558. https://doi.org/10.1016/j.conbuildmat.2018.04.132

Hirschmüller S, Pravida J, Marte R, Flach M (2019) Long-term material properties of circular hollow laminated veneer lumber sections under water saturation and cement alkaline attack. Wood Mater Sci Eng 14:142–156. https://doi.org/10.1080/17480272.2018.1434830

Huybers P (1987) Timber pole space frames. Int J Space Struct 2:77–86

Kang H-Y, Milota M, Kang C, Matsumura J (2011) Preliminary tests for optically measuring drying strains and check formation in wood. J Fac Agric Kyushu Univ 56:313–316

Kollmann F (1955) Technologie des Holzes und der Holzwerkstoffe (Technology of wood and wood-based materials). Springer, Berlin

Langrish TAG, Bohm N (1997) An experimental assessment of driving forces for drying in hardwoods. Wood Sci Technol 31:415–422

Lanvermann C, Sanabria SJ, Mannes D, Niemz P (2014) Combination of neutron imaging (NI) and digital image correlation (DIC) to determine intra-ring moisture variation in Norway spruce. Holzforschung 68:113–122

Lavalette A, Cointe A, Pommier R et al (2016) Experimental design to determine the manufacturing parameters of a green-glued plywood panel. Eur J Wood Prod 74:543–551

Lee SS, Jeong GY (2018) Effects of sample size on swelling and shrinkage of Larix kaempferi and *Cryptomeria japonica* as determined by digital caliper, image analysis, and digital image correlation (DIC). Holzforschung 72:477–488

Lee SS, Pang SJ, Jeong GY (2019) Effects of size, species, and adjacent lamina on moisture-related strain in glulam. Wood Fiber Sci 51:101–118

Makomra V, Oum Lissouck R, Pommier R et al (2020) Analysis of drying stresses in green-glued plywood of Bete (*Mansonia altissima*) specie. J Wood Sci 66:70. https://doi.org/10.1186/s10086-020-01911-1

Nopens M, Riegler M, Hansmann C, Krause A (2019) Simultaneous change of wood mass and dimension caused by moisture dynamics. Sci Rep 9:10309. https://doi.org/10.1038/s41598-019-46381-8

Pang S (2000) Modelling of stress development during drying and relief during steaming in *Pinus radiata* lumber. Drying Technol 18:1677–1696

Pang S-J, Jeong GY (2020) Swelling and shrinkage behaviors of cross-laminated timber made of different species with various lamina thickness and combinations. Constr Build Mater 240:117924. https://doi.org/10.1016/j.conbuildmat.2019.117924

Park JH, Park Y, Han Y et al (2014) Effect of outer surface sealing treatment on the reduction of surface check occurrence during the drying of center-bored round timber. Drying Technol 32:236–243

Peng M, Ho Y-C, Wang W-C et al (2012) Measurement of wood shrinkage in jack pine using three dimensional digital image correlation (DIC). Holzforschung 66:639–643

Pommier R, Guillaume G, Matthieu P, Nordine L (2017) Assembly process for peeled wood in the form of a tube and products issued from this process. French Patent Application Number: FR3052379A1

Pröller M (2016) An investigation into the edge gluing of green Eucalyptus grandis lumber using a one-component polyurethane adhesive. MSc. For (Wood Products Science) thesis. Department of Forest and Wood Science, Stellenbosch University

Properzi M, Pizzi A, Uzielli L (2003) Comparative wet wood gluing performance of different types of Glulam wood adhesives. Eur J Wood Prod 61(1):77–78

Purba CYC, Pot G, Viguier J et al (2019) The influence of veneer thickness and knot proportion on the mechanical properties of laminated veneer lumber (LVL) made from secondary quality hardwood. Eur J Wood Prod 77:393–404

Ranta-Maunus A (1999) Round small-diameter timber for construction. Final report of project FAIR CT 95-0091

Rohumaa A, Viguier J, Girardon S et al (2018) Lathe check development and properties: effect of log soaking temperature, compression rate, cutting radius and cutting speed during peeling process of European beech (*Fagus sylvatica* L.) veneer. Eur J Wood Prod 76:1653–1661

Rosero-Alvarado J, Hernández RE, Riedl B (2018) Surface deformation of walnut burl veneer on aircraft sandwich panels assessed by three-dimensional digital image correlation. Wood Sci Technol 52:1511–1525. https://doi.org/10.1007/s00226-018-1040-z

Ross RJ (2010) Wood handbook: wood as an engineering material. USDA Forest Service, Forest Products Laboratory, General Technical Report FPL-GTR-190, vol 509, pp 1–190

Sepulveda-Villarroel V, Perez-Peña N, Salinas-Lira C et al (2016) The development of moisture and strain profiles during predrying of Eucalyptus nitens. Drying Technol 34:428–436

Shao X, Dai X, Chen Z et al (2016) Calibration of stereo-digital image correlation for deformation measurement of large engineering components. Meas Sci Technol 27:125010. https://doi.org/10.1088/0957-0233/27/12/125010

Stöhr HP (1988) Shrinkage differential as a measure for drying stress determination. Wood Sci Technol 22:121–128

Sutton MA, Orteu JJ, Schreier H (2009) Image correlation for shape, motion and deformation measurements: basic concepts, theory and applications. Springer Science & Business Media

Valla A, Konnerth J, Keunecke D et al (2011) Comparison of two optical methods for contactless, full field and highly sensitive in-plane deformation measurements using the example of plywood. Wood Sci Technol 45:755–765

Viguier J, Marcon B, Butaud JC et al (2021) Panel shear of plywood in structural sizes—assessment improvement using digital image correlation. Exp Tech 45:195–206